Journal of Physics D: Applied Physics

PAPER • OPEN ACCESS

Metamaterial control of the surface acoustic wave streaming jet

OPEN ACCESS
IOP Publishing

Journal of Physics D: Applied Physics

J. Phys. D: Appl. Phys. **57** (2024) 195303 (6pp)

https://doi.org/10.1088/1361-6463/ad2563

Metamaterial control of the surface acoustic wave streaming jet

C Pouya and G R Nash*

Natural Sciences. Faculty of Environment, Science and Economy, University of Exeter, Exeter, United Kingdom

E-mail: g.r.nash@exeter.ac.uk

Received 24 July 2023, revised 30 November 2023
Accepted for publication 2 February 2024
Published 15 February 2024

Abstract

The phenomenon of surface acoustic wave (SAW) streaming, where a streaming jet is created, occurs when an SAW propagating on the surface of a solid interacts with water, and underpins the increasingly important area of SAW microfluidics. A key characteristic of the streaming jet is the Rayleigh angle, i.e. the angle at which the jet is formed relative to the surface normal of the solid, which is determined by the ratio of the velocity of the acoustic wave in the fluid and in the solid. Although the ability to dynamically tune this angle would offer a novel tool for microfluidic control, the SAW velocity is normally fixed by the characteristics of the solid and liquid material properties. In this paper we show, using finite element method modelling, that changing the SAW Rayleigh wave phase velocity by patterning a metamaterial array, consisting of square annular holes, onto the surface of an SAW device can change the acoustic streaming Rayleigh angle by approximately a factor of two, in good agreement with calculations based on the change in velocity.

Supplementary material for this article is available online

Keywords: surface acoustic wave, metamaterials, Rayleigh angle, SAW streaming

1. Introduction

Over the last decade, or so, surface acoustic wave (SAW) devices have had a growing presence in the field of microfluidics [1, 2] due to the phenomenon of acoustic streaming [3], where SAWs can be used to induce fluid motion. When a water droplet is applied to the surface of an SAW device, the propagating SAWs are converted into 'leaky SAWs', which are radiated into the liquid and decay, causing fluid motion [4, 5]. Applications of acoustic streaming include cell sorting [6], SAW swimming [7, 8], microfluidic mixing [9], among many others [10]. Increasingly, SAW streaming is also being explored for the manipulation of nanoparticles [11, 12], with the aim of developing reliable methods for their separation, concentration and purification.

An important parameter that defines the characteristics of the acoustic streaming jet is the Rayleigh angle (θ_R), as shown schematically in figure 1, which can be approximated using Snell's law as;

$$\theta_R = \sin^{-1}\frac{v_f}{v_{SAW}}, \tag{1}$$

where v_f is the velocity of the acoustic wave in the fluid and v_{SAW} is the SAW velocity and θ_R is measured from the surface normal of the SAW device (see figure 1).

When using standard SAW substrates, the material parameters governing the Rayleigh angle (equation (1)) are often fixed for a given wave frequency and so the acoustic jet produced in the liquid propagates at a fixed angle. For instance, when using a material such as lithium niobate (128° YX $LiNbO_3$, v_{SAW} = 3998 ms^{-1} [13]) to induce SAW motion, and applying liquid water (v_f = 1480 ms^{-1}) to the surface, the Rayleigh angle can be calculated to be approximately 22°. The

* Author to whom any correspondence should be addressed.

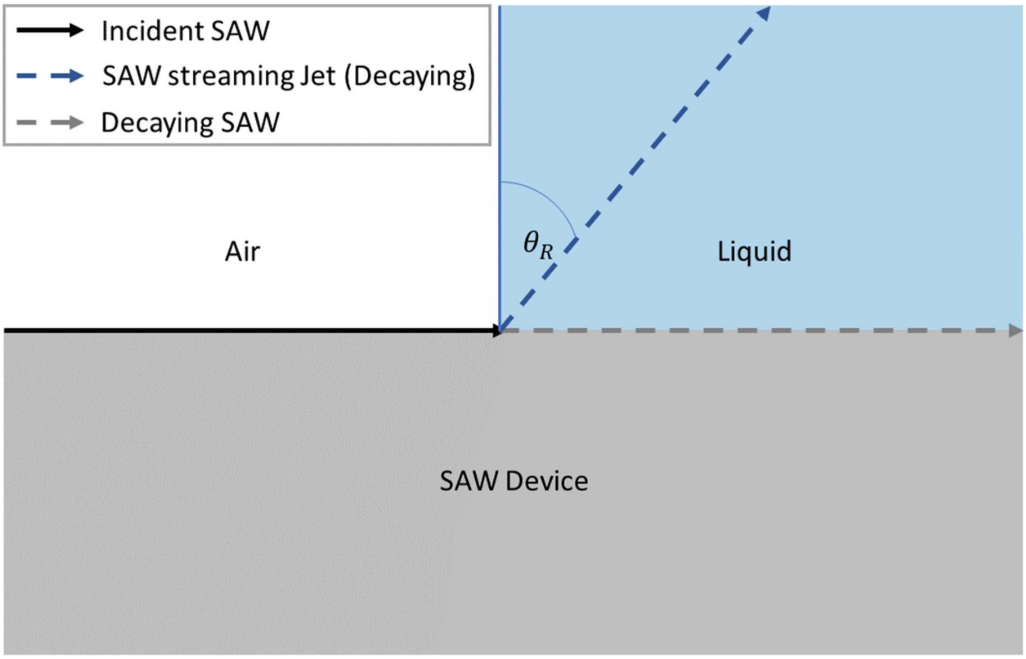

Figure 1. Schematic showing the propagation of an SAW on a device when in contact with a liquid, and a resulting SAW streaming jet.

ability to dynamically control the Rayleigh angle would offer a new tool for the control of SAW streaming and microfluidic processes, and one recent study using plate modes utilised their behaviour and different phase velocities and frequencies to achieve enhanced acoustic streaming for microfluidic mixing [14].

In the work presented here we show that a phononic metamaterial can be used to control the Rayleigh angle of the streaming jet. Metamaterials are a new class of artificial material that can be engineered to possess properties that do not exist in natural materials, and have been increasingly used to control and manipulate the propagation of phonons, including SAWs, at the micro- and nano-scales [15].

We recently demonstrated [16], using simulations and experiment, that the metamaterial patterning on a lithium niobate substrate allows control of SAW phase velocities to values slower and faster than the value of velocity in an unpatterned substrate. By changing the frequency of the SAW, velocities of ∼85% and ∼130% of the unpatterned SAW velocity could be achieved, due to the excitation of different modes within the metamaterial array. In this work we build on this result to show how a reduction in the phase velocity of a lithium niobate device, brought about by metamaterial patterning, in the presence of water can be used to dynamically control the SAW Rayleigh angle.

2. Results and discussion

2.1. Finite element simulations

Using the finite element modelling software package COMSOL Multiphysics® [17], as shown in figure 2, the Rayleigh angle for a lithium niobate (128° YX $LiNbO_3$) block in water was analysed with and without metamaterial patterning. The lithium niobate slab was assigned a solid mechanics domain and electrostatics domain, as a piezoelectric material with piezoelectric multiphysics applied. This is the grey region in figure 2(c).

The patterned array (patterned with the Array#1 geometry described in [16]) had a unit cell size of $a = 8.4$ μm, annulus hole depth $d = 4.95$ μm, annulus hole width $r_w = 1$ μm, and the internal square length dimension of $r_i = 5.5$ μm shown in the inset of figure 2(b). We have previously shown [16] that this annular hole geometry can lead to SAW phase velocities slower and faster than the velocity in an unpatterned substrate (∼85% and ∼130% of the unpatterned SAW respectively). The reduction or increase in phase velocity originated from the dispersion properties of the metamaterial, the modes to which the SAW can couple at a particular frequency and the displacements induced by local resonators within the array. Slow SAWs were achieved as a result of the excitation of the resonators, slowing the propagation of the SAW [16]. However, this previous study was performed without water and experiments were performed in air. In the work presented here, new modelling was undertaken, adding water to the annular holes and above the device.

To identify an SAW frequency suitable for further analysis, a new eigenfrequency study was first performed, including the geometry of the square annulus metamaterial with water in the annular hole region and on the surface of the device (as shown in supplementary figure 1). Supplementary note 1 describes how the mode to be further analysed, with a frequency of 92.5 MHz, was identified. From this eigenfrequency

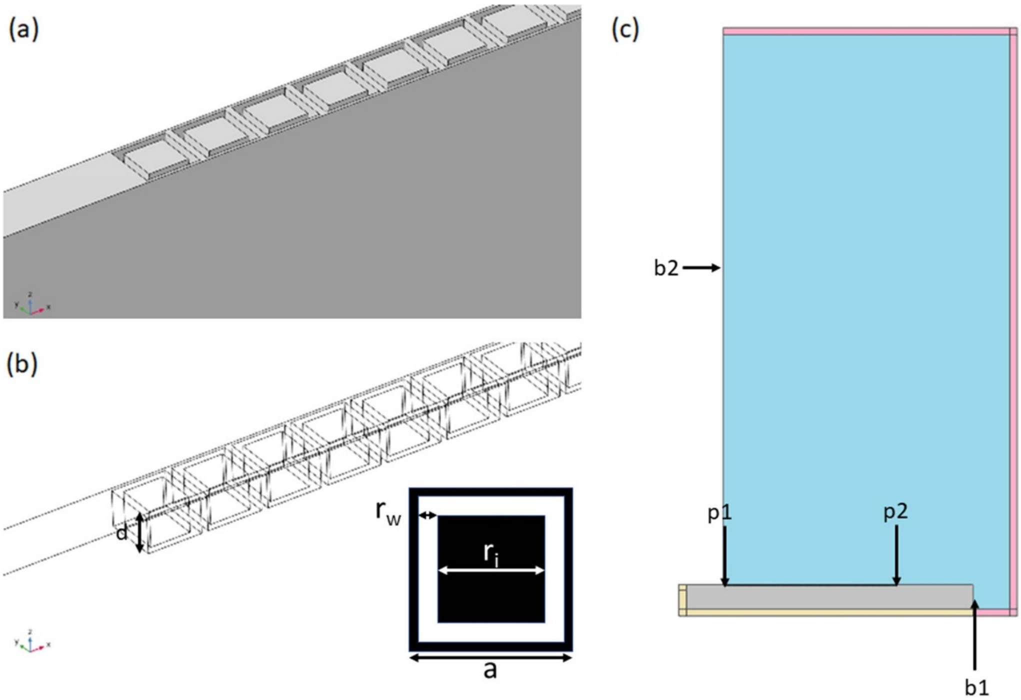

Figure 2. 3D finite element method (COMSOL Multiphysics® [17]) modelling schematics: (a) (b) the lithium niobate device geometry in solid and wireframe perspectives, respectively. (b) Inset shows the annulus geometry. (c) The full modelled geometry (side view) including water (blue), lithium niobate/array (grey), lithium niobate/solid mechanics PML (yellow) and water/pressure acoustics PML (pink) regions.

study, excitation of this mode was predicted to increase the Rayleigh angle to approximately 35°, due the associated change in phase velocity (supplementary figure 2 shows the dispersion, phase velocity and predicted Rayleigh angle from the eigenfrequency study of the selected mode under analysis).

To investigate the SAW streaming jet Rayleigh angle when this mode is excited in the metamaterial, a frequency domain study was then undertaken using the geometry shown schematically in figure 2(c), and at a frequency of 92.5 MHz. For the frequency domain study of a finite system, the lithium niobate slab dimensions were 2 mm $\times$ a $\times$ 0.168 mm. The patterned array was 1 $\times$ 144 unit cells in length, and an SAW was excited on the lithium niobate by using an edge load positioned across the width of the device, three wavelengths away from the first element of the array. The array begins in the water region, approximately position p1 in figure 2(c) and the end of the array is approximately at position p2 in figure 2(c). The edge load was also positioned three wavelengths away from the edge of the device and associated perfectly matched layer (PML) edge. The incident region was unpatterned and was positioned outside of a water domain (the water domain is shown by the blue region in figure 2(c)). The lithium niobate slab was many wavelengths deep and on the base of the lithium niobate domain was a PML, to reduce unwanted reflections. The PML had a fixed constraint boundary applied to the base to avoid exciting any Lamb waves. A PML was also used on the side of the lithium niobate that was positioned outside of the water domain, to reduce further unwanted reflections from the side of the device. The lithium niobate device had a low-reflecting boundary at the opposing end, within the water domain, to minimise reflections from the edge of the finite device (boundary b1 in figure 2(c)). A periodic boundary condition (Floquet) covering the two parallel sides on either side of all regions of the lithium niobate device and the solid mechanics domain in the plane of figure 2(c) was assigned to reduce the model size.

Additionally, an unpatterned lithium niobate slab, was also modelled with the same configuration, but with the patterning removed for comparison.

The water domain dimensions were 2 mm $\times$ a $\times$ 4 mm. This fluid region was assigned as a pressure acoustics domain. An acoustic-structure multiphysics boundary was used at the boundary of the two regions (i.e. the pressure acoustics and solid mechanics domains).

The water region had PMLs surrounding the outside boundaries (the pink regions in figure 2(c)) to reduce the size of the model and to minimise spurious boundary reflections. A sound soft boundary condition was in place at boundary b2 (figure 2(c)). A periodic boundary condition (Floquet) covering the two parallel sides on either side of all regions of the pressure acoustics domain in the plane of figure 2(c) was assigned to reduce the model size.

The mesh resolutions were chosen to have a *maximum* size of $\frac{v_{\mathrm{SAW}}}{8\times 92.5\ [\mathrm{MHz}]}$ for the device and $\frac{v_{\mathrm{f}}}{5\times 92.5\ [\mathrm{MHz}]}$ for the water domain in order to obtain good resolutions of the waves in the solid device and the water region. The minimum mesh size was chosen to be 0.5 μm, in order to obtain a good resolution in the annular hole regions. In the PML regions, a swept mesh with eight layers was used.

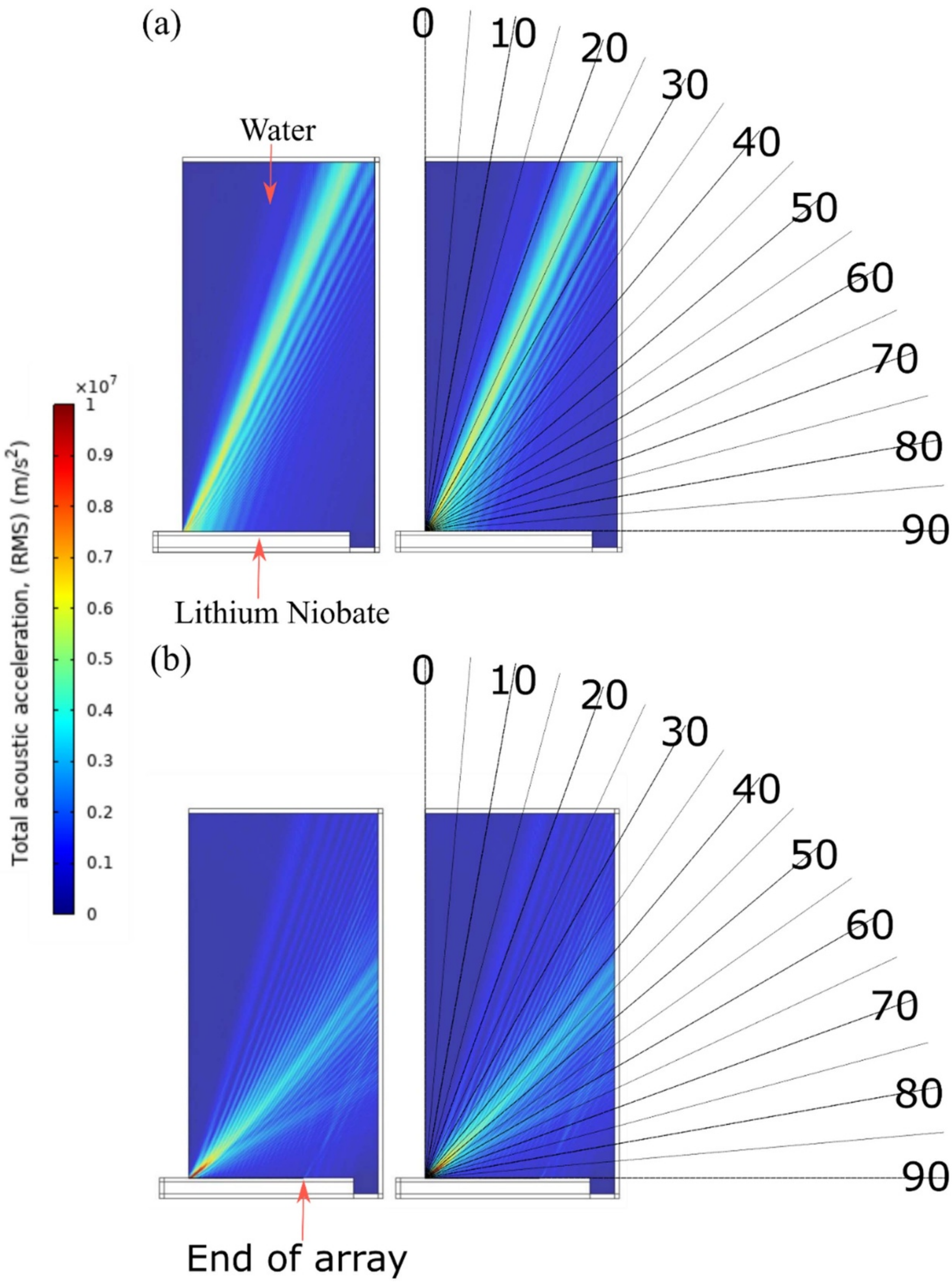

Figure 3. COMSOL Multiphysics® [17] modelling data showing the total acoustic acceleration (RMS) in the water region produced by (a) unpatterned lithium niobate and (b) the square annular hole array patterned onto lithium niobate. Figures on the right are replicated from the left-hand figures with additional angular guides.

Note that the mode shape identified from eigenfrequency analysis (see supplementary figure 3) is also present in the frequency domain modelling results (see supplementary figure 4), confirming that this mode is being excited in both models and thus a comparison between the eigenfrequency and frequency domain models (and their corresponding data) can be made. However, due to the inherent differences between modelling a single unit cell for an eigenfrequency study, and modelling a more realistic finite system as a frequency domain study model, some differences are expected between the predicted SAW behaviour and propagation of the two systems (see supplementary note 1b).

Figure 3 shows the simulated acceleration within the water region caused by SAW acoustic streaming, at an SAW frequency of 92.5 MHz, with the presence of an acoustic jet shown by the regions of high acceleration. Figure 3 is obtained from a frequency domain study. Figures 3(a) and (b) show the results for the unpatterned lithium niobate device and for a device incorporating the metamaterial, respectively. The left- and right-hand figures show the modelled data without and with angle guidance lines, respectively. Figures 3(a) and (b) show the distinct change in Rayleigh angle of the acoustic jet for the unpatterned and patterned systems. This difference is due to the change in phase velocity tailored by metamaterial patterning, and the dependence of equation (1) on the SAW phase velocity. For reference, supplementary figure 5 shows the solid displacement magnitude in the SAW substrate for the unpatterned and patterned devices.

The directional properties of the jet are not entirely linear, particularly close to the source, and also the jet has an associated beam spread [18], and so a clear and distinct value for Rayleigh angle was not easily obtainable, however figure 3(a) shows that the jet predominantly lies between the guides at 20°–30°. This is in-keeping with the estimated value of ∼22° calculated from equation (1).

From figure 3(b), an estimate for the Rayleigh angle of the jet produced from the metamaterial geometry patterned onto lithium niobate from finite element method modelling is approximately between 35° and 50°, where the jet predominantly lies in-between the guides in figure 3(b). As with the unpatterned material, this patterned device produces a jet that has a directionality which is not linear across the length of the jet, particularly close to the source, and has an associated beam spread.

To calculate an equivalent predicated value of the Rayleigh angle from equation (1) for the substrate incorporating the metamaterial array and water, an estimated value of phase velocity can be determined from supplementary figure 2(c) at the frequency of interest, i.e. at 92.5 MHz. Supplementary figure 2(c) shows that this is predicted to produce an acoustic jet with a new metamaterial-induced Rayleigh angle of around 35°, in good agreement with the frequency domain study modelling result presented in figure 3(b), given the angle spread and non-linear appearance. Additionally, a thermoviscous acoustics domain or boundary was not added to the model, but could be added to further investigate the effects with thermoviscous losses. Although the full thermoviscous physics study is very computationally demanding, an approximation of this can be made when the thermoviscous boundary layer is smaller than the minimum feature size, or when the boundary layers are not overlapping, using a thermoviscous boundary layer impedance boundary in the pressure acoustics domain [19]. Results from this initial study, with a reduced water domain size for computational efficiency, are shown in supplementary figure 6, where a thermoviscous boundary layer impedance boundary replaced the acoustic-structure multiphysics coupling boundary and the water domain is considered to be thermally conducting and viscous. The same Rayleigh angles resulted, but with a more gradual jetting across the SAW surface (see supplementary figure 6). Additionally, some reflections occurred in the water region for the metamaterial case. For the model description of this, see supplementary figure 7.

Finally, further work is underway to fabricate a device, with the design based on the results of this modelling study, to demonstrate experimentally the effect of the metamaterial on the SAW streaming jet.

3. Conclusion

Finite element method modelling was used to investigate the effect on the SAW streaming jet, specifically the Rayleigh angle, when the surface of the solid on which the SAW is propagating is patterned with a metamaterial. The geometry studied consisted of an array of square annular holes, submerged in water, in which slower SAW phase velocities can be achieved relative to an unpatterned substrate. Eigenfrequency study modelling was first undertaken to ascertain the response of the structure in the presence of water, and dispersion data predicted the formation of a band, relating to a resonant mode of the array elements, with a reduced SAW phase velocity compared with the Rayleigh wave speed. Further frequency domain simulations of a more realistic system showed that the metamaterial patterning increases the Rayleigh angle by approximately a factor of two compared to the unpatterned case. This proof-of-principle simulation demonstrates that under careful design of a metamaterial geometry, due to the ability to engineer the dispersion characteristics of metamaterials and utilising the frequency dependent properties of a metamaterial rather than a traditional material, the Rayleigh angle of the jet could be tuned using the SAW frequency, potentially offering a new tool for tailored designs of SAW microfluidic devices. Such frequency-tuneable microfluidic and lab-on-a-chip devices could create new approaches for applications such as microfluidic mixing, SAW swimming, and nanoparticle manipulation.

Data availability statement

All data that support the findings of this study are included within the article (and any supplementary files).

Acknowledgments

The authors acknowledge financial support from the Leverhulme Trust (Grant No. RPG-2017-60), and the Engineering and Physical Sciences Research Council of the United Kingdom (A-Meta: A UK–US Collaboration for Active Metamaterials Research, Grant No. EP/W003341/1).

ORCID iDs

C Pouya https://orcid.org/0000-0001-5455-9924
G R Nash https://orcid.org/0000-0002-5321-4163

References

[1] Friend J and Yeo L Y 2011 Microscale acoustofluidics: microfluidics driven via acoustics and ultrasonics *Rev. Mod. Phys.* **83** 647
[2] Ding X *et al* 2013 Surface acoustic wave microfluidics *Lab Chip* **13** 3626
[3] Nyborg W 1996 *Physical Acoustics* ed W P Mason (Academic) pp 265–331

[4] Shiokawa S, Matsui Y and Moriizumi T 1989 Experimental study on liquid streaming by SAW *Jpn. J. Appl. Phys.* **28** 126

[5] Shiokawa M Y and Ueda T 1989 Liquid streaming and droplet formation caused by leaky Rayleigh waves *Proc. Ultrason. Symp.* **641** 643

[6] Franke T, Braunmüller S, Schmid L, Wixforth A and Weitz D A 2010 Surface acoustic wave actuated cell sorting *Lab Chip* **10** 789

[7] Bourquin Y and Cooper J M 2013 Swimming using surface acoustic waves *PLoS One* **8** e0042686

[8] Pouya C, Hoggard K, Gossage S H, Peter H R, Poole T and Nash G R 2019 Frequency dependence of surface acoustic wave swimming *J. R. Soc. Interface* **16** 20190113

[9] Frommelt T, Kostur M, Schäfer M, Talkner P, Hänggi P and Wixforth A 2008 Microfluidic mixing via acoustically driven chaotic advection *Phys. Rev. Lett.* **100** 034502

[10] Yeo L Y and Friend J R 2014 Surface acoustic wave microfluidics *Annu. Rev. Fluid Mech.* **46** 379

[11] Collins D J, Ma Z, Han J and Ai Y 2017 Continuous micro-vortex-based nanoparticle manipulation via focused surface acoustic waves *Lab Chip* **17** 91

[12] Hettiarachchi S, Cha H, Ouyang L, Mudugamuwa A, An H, Kijanka G, Kashaninejad N, Nguyen N-T and Zhang J 2023 Recent microfluidic advances in submicron to nanoparticle manipulation and separation *Lab Chip* **23** 982

[13] Slobodnik A J and Conway E D 1974 Microwave acoustics handbook vol 1. Surface wave velocities *J. Acoust. Soc.* **56** 1307

[14] Hsu J C and Chang C Y 2022 Enhanced acoustofluidic mixing in a semicircular microchannel using plate mode coupling in a surface acoustic wave device *Sens. Actuators* A **336** 113401

[15] Ma J 2023 Phonon engineering of micro- and nanophononic crystals and acoustic metamaterials: a review *Small Sci.* **3** 2200052

[16] Pouya C and Nash G R 2021 Sub and supersonic elastic waves in an annular hole phononic metamaterial *Commun. Mater* **2** 55

[17] COMSOL Multiphysics® v 6.1 2022 (available at: www.comsol.com) (COMSOL AB)

[18] Dentry M B, Yeo L Y and Friend J R 2014 Frequency effects on the scale and behavior of acoustic streaming *Phys. Rev.* E **89** 013203

[19] Acoustics Module User's Guide 2022 COMSOL Multiphysics® v 6.1 (COMSOL AB) p 124